Gambhir reviews the use of aptamers as novel imaging probes and previews an article in this issue of *JNM* on tumor targeting in a small-animal model. . . . . ***Page 557***

Prévost and colleagues evaluate the effectiveness of ^{18}F-FDG PET measures of diffuse bone marrow hypermetabolism and other factors in predicting outcomes in patients with non–small cell lung cancer. . . . . ***Page 559***

Meisetschläger and colleagues compare the pharmacokinetics, biodistribution, and diagnostic performance of a recently introduced ^{18}F-labeled PET tracer for somatostatin receptor (sstr) imaging with ^{111}In-DTPA-octreotide in a population of patients with sstr-positive tumors. . . . . ***Page 566***

Beeres and colleagues use both ^{99m}Tc-tetrofosmin SPECT and ^{18}F-FDG SPECT to investigate the effects of autologous bone marrow–derived mononuclear cell injection into the myocardium of patients with drug-refractory ischemia. . . ***Page 574***

Moore and colleagues apply whole-body and static γ-camera imaging to evaluate the accuracy of measurements of whole-skeleton ^{99m}Tc-MDP plasma clearance obtained using the area-under-the-curve method. . . . . ***Page 581***

Bar-Shalom and colleagues explore the role of SPECT/CT as an adjunct to ^{67}Ga scintigraphy or ^{111}In-labeled white blood cell scintigraphy for diagnosis or localization of suspected infection. . . . ***Page 587***

Funk and colleagues report on a novel multipinhole collimator to improve detection efficiency in cardiac SPECT and detail significant advantages over rotational SPECT with conventional parallel-hole collimators. . . . . ***Page 595***

Engles and colleagues describe a transient "stunning" effect after chemotherapy for breast cancer and discuss potential implications for ^{3}H-FDG PET imaging. . . . . ***Page 603***

Choi and colleagues assess whether ^{18}F-FDG uptake patterns and CT findings improve accuracy over standardized uptake values alone in differentiating benign from malignant focal thyroid lesions incidentally found on ^{18}F-FDG PET/CT. . . . . ***Page 609***

Palmedo and colleagues document the diagnostic accuracy and effect on patient management of PET/CT in patients with suspected iodine-negative, differentiated thyroid carcinoma and compare these results with those obtained by side-by-side interpretation of PET and CT images. . . . . ***Page 616***

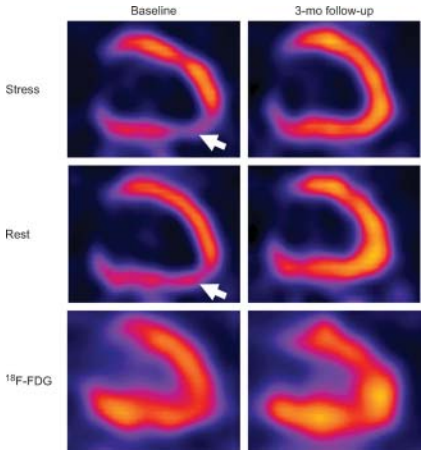

Dumarey and colleagues investigate the feasibility and potential role of PET/CT with ^{18}F-FDG–labeled autologous leukocytes in the diagnosis and localization of infectious lesions in patients with suspected or documented bacterial infections or with fevers of unknown origin. . . . . ***Page 625***

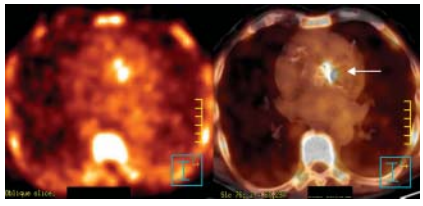

Nishiyama and colleagues evaluate the efficacy of dual-time-point ^{18}F-FDG PET imaging for differentiating malignant from benign gallbladder disease and discuss the limitations and benefits of this approach. . . . . ***Page 633***

Pichler and colleagues describe the initial development of a lutetium oxyorthosilicate–avalanche photodiode array detector PET module to be combined with a 7-T MRI system for high-resolution PET/MRI in small animals. . . . . ***Page 639***

Hänscheid and colleagues report on an international study of postoperative radioiodine ablation therapy with 3.7 GBq of ^{131}I in differentiated thyroid cancer after stimulation with recombinant human thyroid-stimulating hormone or after thyroid hormone withdrawal. . . . . ***Page 648***

Stabin and colleagues provide dose factors for internal sources in realistic, segmented, voxel-based models of a typical

mouse and typical rat, based on image data obtained using a dedicated small-animal CT scanner. . . . . ***Page 655***

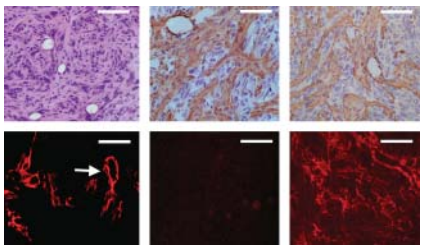

Madsen and colleagues devise a theoretical model to investigate the potential incremental value of combined-agent ^{131}I-MIBG and ^{90}Y-DOTATOC therapy in neuroendocrine tumors. . . . . ***Page 660***

Hicke and colleagues describe a novel approach to assess whether aptamers, small oligonucleotides with the potential to bind tightly to targeted molecules, have potential for in vivo delivery of radioisotopes or cytotoxic agents. . . . . ***Page 668***

Tsukada and colleagues compare the tumor imaging capabilities of the L- and D-isomers of ^{11}C-CMT and ^{18}F-FMT with corresponding ^{11}C-MET isomers and discuss the potential implications of their results for imaging of cerebral and peripheral tumors. . . . . ***Page 679***

Welch and colleagues report on a study to determine whether kinetic modeling in conjunction with small-animal PET can noninvasively quantify alterations in myocardial perfusion and substrate metabolism in a rat model. . . . . ***Page 689***

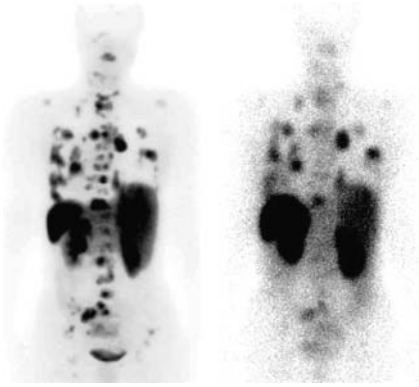

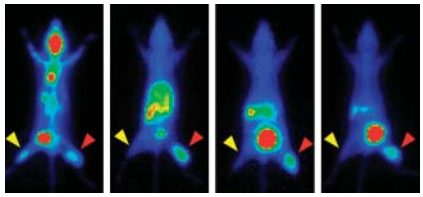

Ametamey and colleagues evaluate ^{11}C-ABO688, a novel antagonist for the metabotropic glutamate receptor subtype 5, as a PET imaging agent in a mouse brain model and point to potential applications in diagnosis and therapy. . . . . ***Page 698***

Yaghoubi and colleagues present the results of a toxicity evaluation of FHBG, which, when labeled with ^{18}F, is a sensitive and specific PET reporter probe for imaging hepatocellular cancer and has been approved as an Investigational New Drug. . . . . ***Page 706***

Kelly and colleagues explore the biodistribution and therapeutic efficacy of a combined ^{90}Y-labeled monoclonal antibody and paclitaxel regimen in a mouse model of breast cancer. . . . . ***Page 716***

ON THE COVER

A 58-y-old patient who had been treated 2 y earlier with total thyroidectomy and ablative radioiodine for oxyphilic follicular thyroid carcinoma presented with a markedly elevated thyroglobulin level but no iodine accumulation. Fine-needle aspiration biopsy of a suggestive cervical lymph node revealed tumor cells. Preoperative PET showed intense ^{18}F-FDG uptake in that lymph node, as demonstrated in a coronal slice (top). However, on a transverse slice (second from top), PET detected a second tumor that was more caudal and for which the CT image (third from top) revealed no corresponding abnormality. Only by fusion of the PET and CT images (bottom) could the second tumor be precisely localized and surgically removed.

SEE PAGE 621